Novel Polygonal Vanadium Oxide Nanoscrolls as Stable Cathode for Lithium Storage

*Qiulong Wei, Shuangshuang Tan, Xiaoyi Liu, Mengyu Yan, Fengchao Wang, Qidong Li, Qinyou An, Ruimin Sun, Kangning Zhao, Hengan Wu, and Liqiang Mai**

Scroll-shape structures with adjustable space provide interlayer sliding to accommodate the volume changes, which are promising candidates for increasing the stability of lithium batteries (LBs). In this work, for the first time, novel vanadium oxide polygonal nanoscrolls (PNSs) are synthesized in solution through self-rolling, Ostwald ripening, and scroll-by-scroll processes. The PNSs are of various shapes (including triangle, quadrangle, pentagon, and so forth) and spiral-wrapped multiwall. When evaluated as cathode for LB, the vanadium oxide PNSs cathode exhibits largely enhanced cycling stability (capacity retention of 91.7% after 150 cycles at 0.1 A g^{-1} in 2.0–4.0 V) compared with those of nonscrolled nanobelts (40.0%) and nanowires (35.8%). Even at 1.0 A g^{-1}, the PNSs cathode delivers high-rate long-life performance with capacity retention of 80.6% after 500 cycles. The unique polygonal nanoscroll structure is favorable for improving the cyclability and rate capability in energy storage applications as demonstrated here, and it will be interesting and has great potential for other related applications.

1. Introduction

Rechargeable lithium batteries (LBs) are rapidly developed for wide applications ranging from mobile electronics to electric vehicles and renewable energy storage.[1–5] One of the key issues is that the active materials of LB will expand/shrink during the repeated ions insertion/extraction, leading to the structure degradation and then the capacity fading.[3–6] The scroll-shape structure materials have attracted wide interest over the past decades owing to their unique electrical and optical properties, which exhibit potential applications in energy storage, electro-optical devices, and biotechnology.[6–13] As a functional nanostructure, the scrolls with open ends/edges, hollow interior and adjustable interlayer could provide easy radial expansion by interlayer sliding to buffer the swelling during lithiation and delithiation.[6,14,15] Schmidt and co-workers developed a strain-released rolled-up nanotechnology to prepare SiO_x/SiO_y[3] and Ge/Ti[4] bilayer nanoscrolls, which effectively buffered the swelling stress during Li^+ ions insertion/extraction and enhanced the cycling stability.[5,16]

Vanadium oxides as potential cathode materials with low cost, abundant source, high energy density, and high theoretical capacity (the multielectron reaction is conducive to realizing high capacity above 200 mAh g^{-1}) have been extensively investigated for LBs, compared with the conventional cathode materials.[17–19] However, the poor cycling stability caused by the collapse of the crystalline structure after repeated lithiation/delithiation needs to be solved urgently.[20] In the previous works, introducing nanoscrolls (NSs) in one-dimensional (1D) nanostructures enhanced the accommodation of volume variations and improved the cycling stability.[21] The vanadium oxide/graphene scrolls displayed remarkable rate and cycling stability owing to the robust graphene outer layer and the volume buffered semihollow inner.[22] These demonstrated that constructing stable vanadium oxide nanoscroll structure is an effective strategy to improve the structure stability and cyclability.

For the synthesis of nanoscrolls/rolls structure, various sizes and compositions have been investigated and explained by some detailed rolling mechanisms.[23–31] Generally, the scrolls/rolls can be formed by rolled-up thin nanobelts, nanosheets or nanoribbons under disparate surface stresses on opposite sides of the layers but the shapes were almost circular.[26,27] It is known that the property of nanomaterial is very closely related to their microscopic shapes.[28–33] Ceder and co-workers presented a simulated polygonal nanotube model.[34] The flat section of the polygonal nanotube is coherent interface with no tensile strain when compared with the existence of tensile strain in circular incoherent interface. And the strain energy is concentrated in corners owing to the smaller bending radius, thus the multiwall nanoscroll with polygonal cross-section could have lower energy than that with circular-cross section. However, as a novel shape of NSs, the inorganic polygonal NSs

Q. Wei, S. Tan, M. Yan, Q. Li, Dr. Q. An, R. Sun, K. Zhao, Prof. L. Mai
State Key Laboratory of Advanced Technology for Materials Synthesis and Processing
WUT-Harvard Joint Nano Key Laboratory
Wuhan University of Technology
Hubei, Wuhan 430070, China
E-mail: mlq518@whut.edu.cn

X. Liu, Dr. F. Wang, Prof. H. Wu
CAS Key Laboratory of Mechanical Behavior and Design of Materials
Department of Modern Mechanics
University of Science and Technology of China
Hefei, Anhui 230027, China

Dr. Q. An
Cullen College of Engineering
Department of Electrical and Computer Engineering
University of Houston
Houston, TX, USA

DOI: 10.1002/adfm.201404311

(PNSs) may exhibit some unique properties but the real synthesis is rarely reported.

Herein, for the first time, the multiwall and well-defined vanadium oxide PNSs are synthesized via the self-rolling, Ostwald ripening, and scroll-by-scroll processes in aqueous solution. Such novel scrolls with robust outer wall and expandable inner space would provide stable structure for the volume swelling/shrink during ions insertion/extraction, leading to the long-term cycling stability. When evaluated as LBs cathode, the unique PNSs structure exhibited the largely enhanced cycling stability (capacity retention of 80.6% after 500 cycles at 1.0 A g^{-1} in 2.0–4.0 V), which is largely enhanced than that of the non-scrolled ultrathin nanobelts (UNBs) (27.9%) and nanowires (NWs) (23.0%).

2. Results and Discussion

The PNSs with various shapes (ca. triangle, quadrangle, pentagon, and so forth) are clearly observed in the field-emission scanning electron microscopic (FESEM) images (**Figures 1** and S1, Supporting Information). The thickness of the scrolls ranges from 50 to 150 nm. The high-magnification FESEM images clearly reflect that the PNSs are spiral-wrapped multiwall. Moreover, the coaxial scrolls (scroll-by-scroll) exist in the products (Figures 1f and S2, Supporting Information). The unique structure of PNSs is different from the previous reported nanotubes/nanorolls/nanoscrolls.[8–11,13,35–37] Through rationally improving the concentration of reactants, the UNBs (Figure S3a,b, Supporting Information) were obtained (details in the Experimental Section). Further increasing the reactant concentration, the NWs with tens of micrometers long (Figure S3c,d, Supporting Information) were synthesized. These results suggest that the reaction concentration has significant influence on their final morphologies.

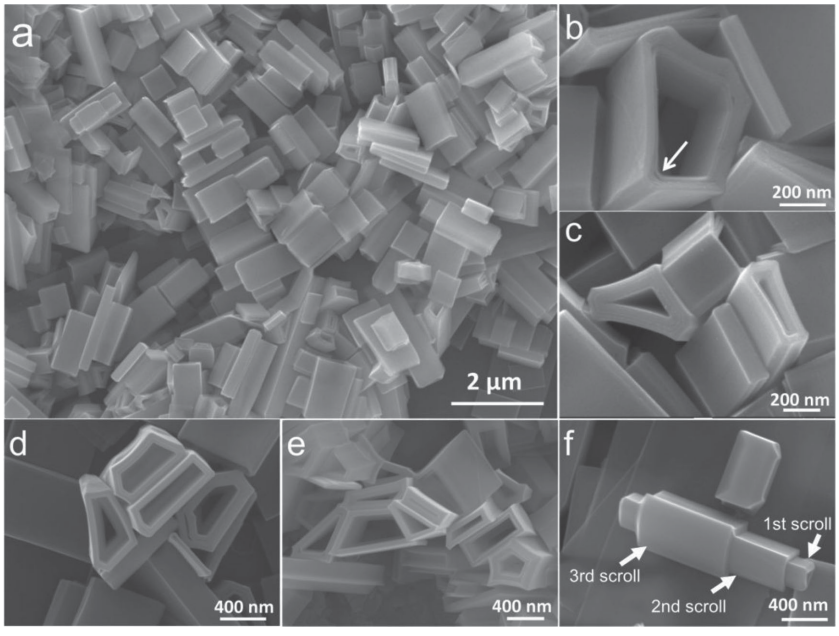

Figure 1. a–f) FESEM images of the as-synthesized PNSs.

The phase of the samples was identified by powder X-ray diffraction with area detector (XRD^2) (**Figure 2**a). All the peaks of the NWs can be indexed to the orthorhombic $H_2V_3O_8$ ($V_3O_7 \cdot H_2O$) (JCPDS No. 85–2401, space group: *Pnam*).[38] However, the PNSs and UNBs mainly exhibit the multiple *(00*l*) reflections, indicating a typical layered structure.[29,33] Two smaller intensity peaks located at 47.5° and 50.0° are corresponding to the (540) and (002) facets of $H_2V_3O_8$. The higher intensity of peak located at 26.22° may be due to an overlapping of *(004) reflection and (011) facets of $H_2V_3O_8$. To confirm the preferred orientation of the samples, 2D XRD spectra at various *psi*-axis angles were collected (Figures S4,S5, Supporting Information). The bright fringes corresponding to *(00*l*) reflections gradually weaken and even disappear with the enlarged degree of *psi*-axis, but the (011) reflection at 26.22° remains (Figure S4, Supporting Information). Meanwhile, for the NWs, all the peaks are almost unchanged with the variation of *psi*-axis (Figure S5, Supporting Information). In addition, the large exposure of *(00*l*) reflection move toward higher angle after drying at 200 °C (Figure S6a, Supporting Information), which is due to the evaporation of absorbed water and organic molecule under this temperature according to the Thermogravimetric analysis (TGA) results (Figure S6b, Supporting Information).[30] These results demonstrate that the crystalline vanadium oxide and the well-orientation of the scrolled/stacked belts.[39]

The crystal structure of $H_2V_3O_8$ consists of V_3O_8 layers, held together by hydrogen bonds.[40] The building blocks for each layer are VO_6 octahedra and VO_5 trigonal bipyramids sharing edges and corners.[41] The samples were further characterized by Fourier transform infrared (FT-IR) and Raman spectra (Figures 2b and S7, Supporting Information). The peak at 3409 cm^{-1} is assigned to the stretching vibration of O–H band. The symmetric band at 1621 cm^{-1} comes from the $\delta(H_2O)$ vibrations, which indicates the existence of water molecules.[41] The peak at 540 cm^{-1} corresponds to the stretching vibrations of the υ_s(V–O–V) bridging bonds. The bands at 1014 and 970 cm^{-1} correspond to the symmetric stretching of the $\upsilon_s(V^{5+}{=}O)$ and $\upsilon_s(V^{4+}{=}O)$ bonds, respectively.[42] However, the symmetric stretching of $\upsilon_s(V^{4+}{=}O)$ and $\upsilon_s(V^{5+}{=}O)$ bonds of the PNSs and the UNBs merge into one peak at 1005 cm^{-1}, which may be due to the different exposed facets and unsaturated bonds between the PNSs/UNBs and NWs (see below discussion) or the influence of the insertion/adsorption of organic and water molecules.[30] The characteristic peak of organic molecule was hardly observed, which may be due to the intense stretching of V–O bonds and the small amount of agent used. The Raman spectra (Figure S7, Supporting Information) show the similar peaks of the three samples, which demonstrates that the same V_3O_8 layer stack behaviors.[43]

The chemical compositions and states of the samples were further characterized by X-ray photoelectron spectroscopy (XPS) (Figure 2c,d). The survey

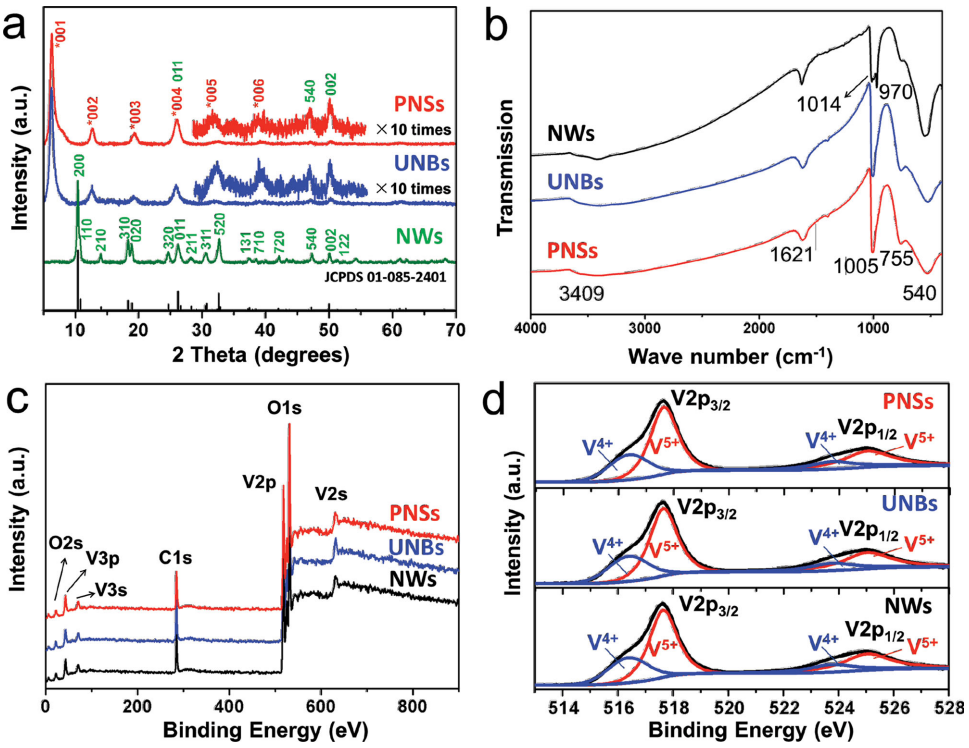

Figure 2. Powder XRD patterns. a) FT-IR spectra; and b) XPS spectrum c,d) of the PNSs, UNBs, and NWs.

spectra (Figure 2c) reveal that the samples consist of vanadium and oxygen. The 2*p* core level spectrum of vanadium displays two asymmetrical peaks related to the V $2p_{3/2}$ and V $2p_{1/2}$ orbital (Figure 2d).[44] The V $2p_{3/2}$ peak could be divided into two peaks, corresponding to V^{5+} (517.8 eV) and V^{4+} (516.2 eV), confirming the mixed valence states of vanadium.[44,45] The V^{5+}/ V^{4+} ratio was calculated from the integration of the V 2*p* peaks. The V^{5+}/V^{4+} ratio of NWs, UNBs, and PNSs are 1.99, 2.01, and 2.02, respectively, which are close to the theoretical value for the $V^{5+}:V^{4+} = 2:1$ of $H_2V_3O_8$. Combining the above results and adding molar ratio of 1,2-propanediol (1,2-PDO):V = 1:5.8, the redox process is described as Equation (1), while the secondary hydroxyl is not oxidized.

$$3V_2O_5 + H_2O + CH_3CHOHCH_2OH \rightarrow 2H_2V_3O_8 + CH_3CHOHCHO \quad (1)$$

Detailed morphology and crystalline structure of the samples were characterized by transmission electron microscopy (TEM) and high-resolution TEM (HRTEM) (**Figures 3** and S8, Supporting Information). The PNSs with multiwalls are clearly observed in Figure 3a. The lattice spacings of 0.47 and 0.34 nm provide the information about crystal structure within the walls of scrolls (Figure 3b), which correspond to the (020) and (011) interplanar distances of $H_2V_3O_8$ (JCPDS No. 85–2401), respectively. The lattice fringe shiftings in the arris are due to the fold of the belt (Figure S9, Supporting Information). The SAED pattern (Figure 3c) reveals the well-defined orientation of the rolled layer and the axial direction of nanoscroll is [020].[29,30,33] The UNBs are ultrathin structures with a few of wrinkles (Figure 3d). When the wrinkle is magnified, layer fringes indicate the lamellar structure. And the thickness of single UNB is ≈4 nm (Figure 3e). The SAED pattern of UNBs indicates the same crystal plane as that of the PNSs (Figure 3f). However, the two sets of reciprocal lattices with a slight rotation are due to the disorderedly stacked UNBs, which is different from that of the ordered rolled scrolls (Figure 3c). The NWs (Figure 3g–i) exhibit a [011] growth direction, indicating the reaction concentration not only influences the morphology but also the growth direction of crystal.

To further investigate the formation process of the PNSs in the solution, time-dependent and control experiments were carried out (Figures S10–S12, Supporting Information). The schematic illustration is shown in **Figure 4**. At the beginning of reaction, nanobelts are obtained (Figure S10a, Supporting Information). Then, the nanobelts self-roll into the polygonal scrolls (Figure S10b, Supporting Information). Next, the scrolls grow along their axial direction to become longer (Figure S10c,d, Supporting Information). Finally, the nanobelts further adsorb onto the scrolls and coil into the multiwall scrolls (Figure 1). On the basis of the demonstrated results above, a probable growth mechanism of the PNSs can be proposed. The strain energy can be expressed as $E_s = YIl/2R^2$ according to a simple beam model[10] (Y is the Young modulus, R is and the radius of the coil, $I = bh^3/12$ is the geometrical moment of inertia of a nanobelt with the width b, thickness h and contour length l). Therefore, the thin nanobelts are flexible and easily self-roll or interattract to reduce their energy state (Figure S10a, Supporting Information).[24,30] In the low concentration, there is more free space for the self-rolling of nanobelts. However, in a higher concentration, the nanobelts tend to attract with each other, resulting in the stacked nanobelts

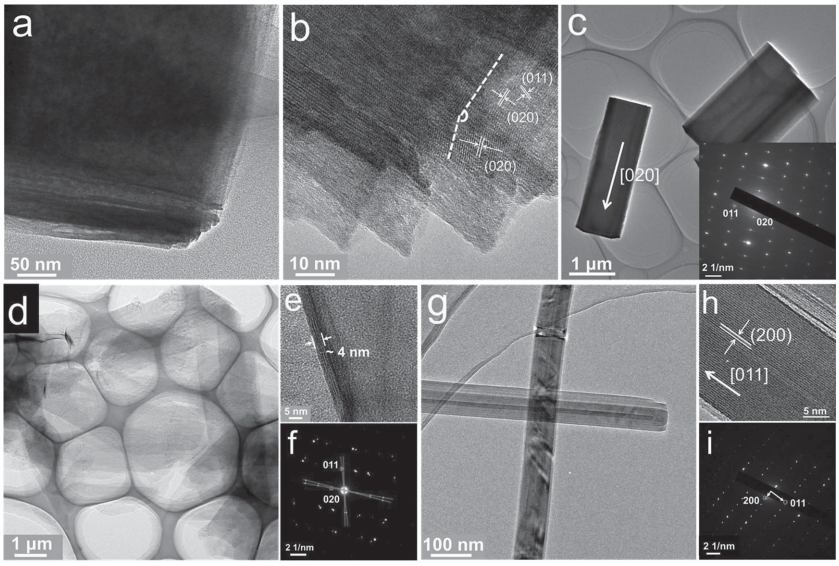

Figure 3. a–c) TEM image; and a) HRTEM image b) of an end of the PNS. c) TEM images of the PNSs, inset is the related SAED pattern of a nanoscroll. d–f) TEM image; d) HRTEM image; and e) SAED pattern f) of the UNBs. g–i) TEM image; g) HRTEM image and h) SAED pattern i) of the NWs.

(Figure S3a,b, Supporting Information). The electrostatic interactions and van der Waals (vdW) attraction between the oxide layer, and the alkanol molecules played an important role in the formation of scrolls.[24] When the nanobelt is rolled, the absorption of surfactant and vdW interaction of V_3O_8 layer would drive the nanobelt to continue coiling. However, owing to the absorption of small alkanol molecule on opposite sides of the belts surface, the overlap of two aggregate ligands in random sites would cause two kinds of strong opposite force (the vdW interaction of the layers and the repulsion of ligand–ligand interactions). The two lopsided forces may lead to the random bending folds. Meanwhile, the redox reaction (Equation (1)) between the V^{5+} and adsorbed –OH leads to an increase of V^{4+}/V^{5+} ratio, which promotes the rearrangement of vanadium oxide crystal and the formation of the bending folds.[24] This crystal rearrangement in the fold (Figures 3b and S9, Supporting Information) is different from the twin crystal boundaries.[46] As demonstrated previously,[34] in a polygonal nanotube/nanoscroll, the most of strain and interfacial energy is located in the corners and the length and location of the flat segments have no effect on the energy. Due to this unique property, the polygon can be distorted/reconfigured with no change in energy, resulting in the various shapes. Along with the reaction, the nanoscroll fast grows along the [020] direction owing to the Ostwald ripening process,[47,48] while the growth direction of [200] is limited due to the absorption of the surfactants on the V_3O_8 layer.[47,49] The molar ratio of surfactant/vanadium is a crucial parameter in the finial morphology.[30] The increased ratios of 1,2-PDO:V influence the distribution of alkanol adsorbed on the oxide layer and their finial morphology (Figure S11, Supporting Information). At last, since the same exposed facets of the nanosrolls and nanobelts, the vdW interactions promote the nanobelts continually adsorbing and coiling, producing the scroll-by-scroll coaxial structure and the back-to-back attraction of PNSs (Figures 1 and S2, Supporting Information).[50]

The species of alkanol molecule in the synthetic system would play an important role in the formation of the finial morphologies (Figure S12 and Table S1, Supporting Information).[29,30,33] To confirm the influence of different small alkanol molecule in rolling process, various experiments utilizing alkanols with different alkyl-chain length and different hydroxyl amount were undertaken. The polygonal-shape scrolls are obtained by using from propyl alcohol (n_C = 3) to hexanol (n_C = 6) (Figure S12a–g, Supporting Information). And circular-shape scrolls are obtained by using octanol (n_C = 8) (Figure S12h, Supporting Information) and cetanol (n_C = 16) (Figure S12i, Supporting Information). As the previous report about the intercalation of alkyl ammonium ions in vanadium oxide layer, small alkyl ammonium ions (n_C < 6) lie parallel to the layer planes, while long chain ions (n_C > 12) remain parallel

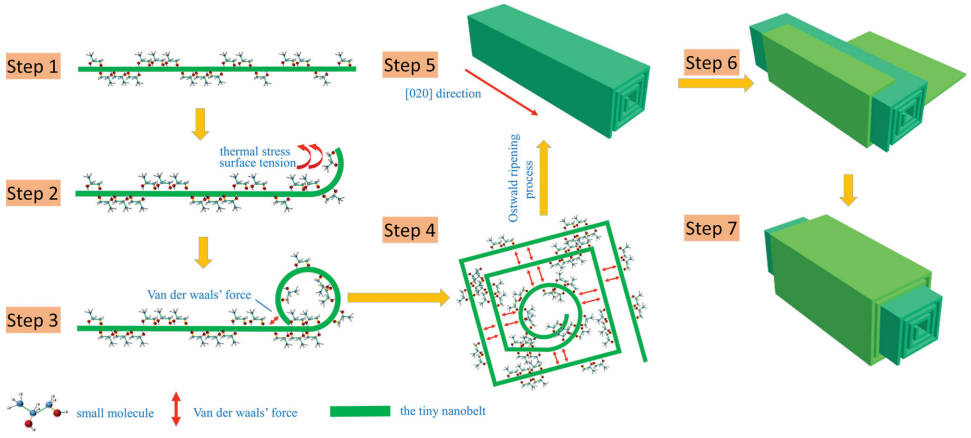

Figure 4. Schematic of the formation process of the PNSs (rectangular scroll as an example), which includes the self-roll, Ostwald ripening, and scroll-by-scroll processes.

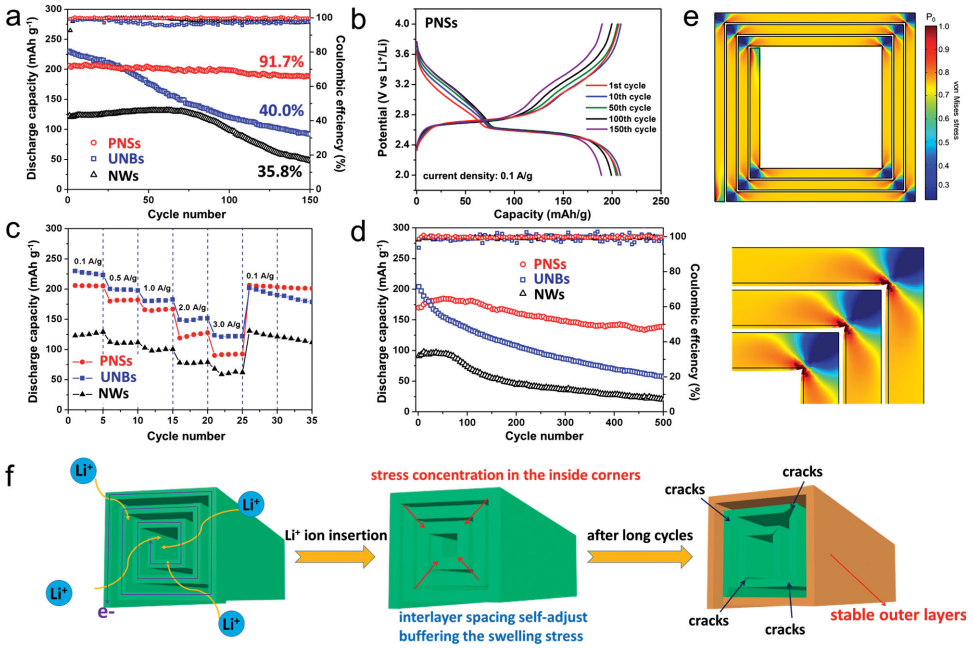

Figure 5. a) Cycling performance of the PNSs, UNBs, and NWs cathodes at 0.1 A g^{-1} in 2.0–4.0 V, and the corresponding coulombic efficiency. b) Charge–discharge curves of the PNSs cathode at 0.1 A g^{-1} in different cycles. c) Rate performance of the cathodes cycled at varied current density in 2.0–4.0 V. d) High-rate and long-life cycles at 1.0 A g^{-1} in 2.0–4.0 V, and the corresponding coulombic efficiency. e) The calculated von Mises stress contour for rectangular nanoscroll. An initial stress P_0 was applied to simulate the diffusion-induced stress resulting from the ion intercalation. The stress concentration can be observed distinctly near the inside corners. f) Schematic of the morphology evolution of the PNSs after cycles.

to each other and perpendicular to the layer planes.[24] The vertical adsorption of long chain alkanol on the belts and the large steric repulsion among the parallel alkane chains counterbalance the strain on the coil surface, resulting in the circular-shape scrolls. However, the small molecular alkanols laying on the nanobelts increase the overlap area as descripted above, promoting the formation of the polygonal-shape scrolls.

Electrochemical lithium storage behaviors for the different structures were investigated by assembling coin cells (2016-type) with metallic lithium as anode. **Figure 5**a shows the discharge capacity of samples at 0.1 A g^{-1} in 2.0–4.0 V. The initial discharge capacity of the PNSs, UNBs, and NWs delivers 206, 230, and 122 mAh g^{-1}, respectively. After 150 cycles, the discharge capacity of the PNSs, UNBs, and NWs is 189 (91.7% of its initial capacity), 92 (40.0% of its initial capacity), and 48 mAh g^{-1} (39.3% of its initial capacity), respectively. The initial discharge capacity of UNBs is higher than that of PNSs owing to the more exposed area of the nonscrolled belts (surface area of 15.78 m^2 g^{-1}) than the PNSs (surface area of 13.09 m^2 g^{-1}, Table S2, Supporting Information). The main discharge plateau of the PNSs was stably located at ≈2.6 V (Figure 5b) during the long-term cycling. But, the UNBs cathode exhibits fast capacity fading along with the shortened plateau at ≈2.6 V (Figure S13a, Supporting Information). However, the NWs exhibits the largest surface area (20.63 m^2 g^{-1}) but the lowest capacity among the three samples. These demonstrate that the capacity based on the ion intercalation reaction mechanism mainly dependeds on their crystal structure instead of the surface area, which is in aggreement with the result by Dunn and co-workers.[51] In the charge–discharge curves (Figure S13b, Supporting Information), the discharge plateaus at ≈2.6 V of the NWs is shorter than the plateaus of the PNSs, UNBs, and previous reports,[38,39] which is probably because that the exposed crystal plane of NWs is different from that of the PNSs and UNBs, leading to the lower capacity.[52]

To evaluate the rate capability, the cathodes were cycled at various rates ranging from 0.1 to 3.0 A g^{-1} (Figures 5c and S14, Supporting Information). The PNSs cathode still delivers a high discharge capacity of 91 mAh g^{-1} at 3.0 A g^{-1}. Even suffering from rapid change of the charge–discharge rates, the cathode exhibits stable capacity at each current. When the current is turned back to 0.1 A g^{-1}, a discharge capacity of 201 mAh g^{-1} is obtained (97.6% of capacity was recovered) and with no obvious capacity decays after the following cycles. However, the UNBs cathode delivers a discharge capacity of 178.6 mAh g^{-1} (77.7% of the initial capacity) when the current is returned. These results indicate the good rate stability of the PNSs. Long-life cycling performance of the samples at high rate up to 1.0 A g^{-1} were tested (Figure 5d). The initial discharge capacity of the PNSs cathode is 170 mAh g^{-1}. And the capacity retention is 80.6% after 500 cycles, much more stable than those of the UNBs (27.9%) and NWs (23.0%), demonstrating the largely enhanced cycling stability of the PNSs.

The electrochemical impedance spectra (EIS) were used to provide further insights (Figure S15, Supporting Information).[20] The Nyquist plots show that the charge transfer resistance (R_{ct}) of the PNSs cathode after 3 cycles is 53.4 Ω, closed to 65.9 Ω for the UNBs and much lower than that of NWs (117.2 Ω). And the impedance increase of PNSs cathode after 10 and 20 cycles are much lower than those of the UNBs and NWs, indicating the stable outer interface of the scrolls during cycling.[53] Further, the morphologies of the cathodes

after cycles are showed in Figure S16 (Supporting Information). The UNB and NW structure are quite different from their morphologies before cycles (Figure S16e,f, Supporting Information), which is due to the repeated volume expansions and shrinks caused destruction. But for the PNSs, the scroll-shapes are largely remained after long-term cycles (Figure S16a, Supporting Information). Some cracks are found on the scroll's inside arris, which may be due to the stress concentration in the process of volume expansion (Figure S16b,c, Supporting Information), but the main polygonal scroll structure is effectively maintained, indicating the robust structure of the polygonal scrolls. Finite element method simulations were carried out to investigate the stress distribution of the PNSs after Li^+ ions intercalation (details are in the Supporting Information), while three kinds of cross-sectional shapes were selected to explain, including rectangle, triangle, and trapezoid (Figures 5e and S17, Supporting Information). Initial stress was applied to simulate the diffusion-induced stress resulting from the ions intercalation. The von Mises stress was calculated and the stress contours were plotted for each model. The stress concentrations are observed distinctly near the inside corners for all the models. Thus, fatigue cracks would occur at the corners firstly, which coincides with the SEM results (Figure S16, Supporting Information). A probable self-limited buffered effect is proposed to explain the largely enhanced cycling stability (Figure 5f).[22,53,54] The interlayer space of scroll would self-adjust to buffer the volume expansion caused by ions insertion. Meanwhile, the sliding is limited by the folds of the polygonal, which aggravates the stress concentration in the corners and then causes the cracks in the inside corners. But the outer walls are not destroyed, which provide the stable electrode–electrolyte interface and long-term cycling stability.[3,4] In addition, the nanobelts scrolled layers offer a continuous transport pathway for electrons, and the hollow of the scrolls provides fast transport channels for Li^+ ions.[22] The thin wall of the scrolls shortens the ion diffusion length, resulting in the good rate performance.[6,21]

3. Conclusion

Polygonal nanoscrolls have been successfully synthesized for the first time via a self-rolling, Ostwald ripening and scroll-by-scroll process in aqueous solution. Various small alkanol molecules ($n_C < 6$) are used as the surfactant to synthesize the polygonal vanadium oxide nanoscrolls and the shape of scrolls is controlled to be circular-shape with the increasing of alkyl chain ($n_C = 8$ to 16), which opens a facile method to synthesize functional nanosrolls with different shapes, adjustable interlayers and so forth. When evaluated as the cathode for LBs, the vanadium oxide PNSs exhibit largely enhanced high-rate cycling stability (capacity retention of 80.6% after 500 cycles at 1.0 A g^{-1} in 2.0–4.0 V) compared with those of the nonscrolled UNBs (27.9%) and NWs (23.0%). The remarkable lithium storage performance of PNSs is due to the robust outer wall and expandable inner space buffered the swelling stress during lithiation/delithiation, resulting in the long-term cycling stability. Meanwhile the thin thickness of scroll's wall reduces the ion diffusion distance, increasing the rate capability. This kind of novel polygonal nanoscroll structure represents an interesting model for the lithium storage here and will exhibit other unique properties for expanding the applications.

Supporting Information

Supporting Information is available from the Wiley Online Library or from the author.

Acknowledgements

Q.L.W. and S.S.T. contributed equally to this work. This work was supported by the National Basic Research Program of China (Grant Nos. 2013CB934103 and 2012CB933003), the National Science Fund for Distinguished Young Scholars (Grant No. 51425204), the National Natural Science Foundation of China (Grant Nos. 51272197, 11172289, and 11472263), the International Science and Technology Cooperation Program of China (Grant No. 2013DFA50840), the Hubei Science Fund for Distinguished Young Scholars (Grant No. 2014CFA035), Anhui Provincial Natural Science Foundation (Grant Nos. 1308085QA10 and 1408085J08), the Fundamental Research Funds for the Central Universities of China (Grant Nos. 2014-YB-001, 2014-YB-002, and WK20900050027), and the Students Innovation and Entrepreneurship Training Program (Grant No. 20141049701006). Thanks to Prof. C. M. Lieber of Harvard University and Prof. D. Y. Zhao of Fudan University for strong support and stimulating discussion.

Received: December 6, 2014
Revised: January 6, 2015
Published online: February 3, 2015

[1] L. Mai, X. Tian, X. Xu, L. Chang, L. Xu, *Chem. Rev.* **2014**, *114*, 11828.
[2] K. Xu, *Chem. Rev.* **2014**, *114*, 11503.
[3] L. Zhang, J. Deng, L. Liu, W. Si, S. Oswald, L. Xi, M. Kundu, G. Ma, T. Gemming, S. Baunack, F. Ding, C. L. Yan, O. G. Schmiddt, *Adv. Mater.* **2014**, *26*, 4527.
[4] C. Yan, W. Xi, W. Si, J. Deng, O. G. Schmidt, *Adv. Mater.* **2013**, *25*, 539.
[5] J. Deng, H. Ji, C. Yan, J. Zhang, W. Si, S. Baunack, S. Oswald, Y. Mei, O. G. Schmidt, *Angew. Chem. Int. Ed.* **2013**, *125*, 2382.
[6] H. X. Ji, X. L. Wu, L. Z. Fan, C. Krien, I. Fiering, Y. G. Guo, Y. Mei, O. G. Schmidt, *Adv. Mater.* **2010**, *22*, 4591.
[7] W. O. Yah, H. Xu, H. Soejima, W. Ma, Y. Lvov, A. Takahara, *J. Am. Chem. Soc.* **2012**, *134*, 12134.
[8] J. Zheng, H. Liu, B. Wu, Y. Guo, T. Wu, G. Yu, Y. Liu, D. Zhu, *Adv. Mater.* **2011**, *23*, 2460.
[9] V. M. Fomin, R. O. Rezaev, O. G. Schmidt, *Nano Lett.* **2012**, *12*, 1282.
[10] P.-P. Wang, Y. Yang, J. Zhuang, X. Wang, *J. Am. Chem. Soc.* **2013**, *135*, 6834.
[11] F. Zeng, Y. Kuang, Y. Wang, Z. Huang, C. Fu, H. Zhou, *Adv. Mater.* **2011**, *23*, 4929.
[12] Q. Huang, S. Hu, J. Zhuang, X. Wang, *Chem. Eur. J.* **2012**, *18*, 15283.
[13] S. Hu, X. Wang, *J. Am. Chem. Soc.* **2008**, *130*, 8126.
[14] A. K. Schaper, M. S. Wang, Z. Xu, Y. Bando, D. Golberg, *Nano Lett.* **2011**, *11*, 3295.
[15] S. F. Braga, V. R. Coluci, S. B. Legoas, R. Giro, D. S. Galvão, R. H. Baughman, *Nano Lett.* **2004**, *4*, 881.

[16] Y. Mei, G. Huang, A. A. Solovev, E. B. Urena, I. Mönch, F. Ding, T. Reindl, R. K. Fu, P. K. Chu, O. G. Schmidt, *Adv. Mater.* **2008**, *20*, 4085.
[17] M. S. Whittingham, *Chem. Rev.* **2004**, *104*, 4271.
[18] J. Yan, A. Sumboja, E. Khoo, P. S. Lee, *Adv. Mater.* **2011**, *23*, 746.
[19] T. Zhai, H. Liu, H. Li, X. Fang, M. Liao, L. Li, H. Zhou, Y. Koide, Y. Bando, D. Golberg, *Adv. Mater.* **2010**, *22*, 2547.
[20] L. Mai, Q. An, Q. Wei, J. Fei, P. Zhang, X. Xu, Y. Zhao, M. Yan, W. Wen, L. Xu, *Small* **2014**, *10*, 3032.
[21] L. Mai, Q. Wei, Q. An, X. Tian, Y. Zhao, X. Xu, L. Xu, L. Chang, Q. Zhang, *Adv. Mater.* **2013**, *25*, 2969.
[22] M. Yan, F. Wang, C. Han, X. Ma, X. Xu, Q. An, L. Xu, C. Niu, Y. Zhao, X. Tian, *J. Am. Chem. Soc.* **2013**, *135*, 18176.
[23] T. Sharifi, E. Gracia-Espino, H. R. Barzegar, X. Jia, F. Nitze, G. Hu, P. Nordblad, C.-W. Tai, T. Wågberg, *Nat. Commun.* **2013**, *4*, 2319.
[24] M. Jaber, F. O. Ribot, L. Binet, V. R. Briois, S. Cassaignon, K. Rao, J. Livage, N. Steunou, *J. Phys. Chem. C* **2012**, *116*, 25126.
[25] G. Shen, D. Chen, *J. Am. Chem. Soc.* **2006**, *128*, 11762.
[26] O. G. Schmidt, K. Eberl, *Nature* **2001**, *410*, 168.
[27] S. Zhang, L.-M. Peng, Q. Chen, G. Du, G. Dawson, W. Zhou, *Phys. Rev. Lett.* **2003**, *91*, 256103.
[28] S. A. Corr, M. Grossman, J. D. Furman, B. C. Melot, A. K. Cheetham, K. R. Heier, R. Seshadri, *Chem. Mater.* **2008**, *20*, 6396.
[29] F. Krumeich, H.-J. Muhr, M. Niederberger, F. Bieri, B. Schnyder, R. Nesper, *J. Am. Chem. Soc.* **1999**, *121*, 8324.
[30] D. McNulty, D. N. Buckley, C. O'Dwyer, *J. Power Sources* **2014**, *267*, 831.
[31] X. Chen, X. Sun, Y. Li, *Inorg. Chem.* **2002**, *41*, 4524.
[32] T. J. Kempa, R. W. Day, S.-K. Kim, H.-G. Park, C. M. Lieber, *Energy Environ. Sci.* **2013**, *6*, 719.
[33] M. Niederberger, H.-J. Muhr, F. Krumeich, F. Bieri, D. Günther, R. Nesper, *Chem. Mater.* **2000**, *12*, 1995.
[34] K. Tibbetts, R. Doe, G. Ceder, *Phys. Rev. B* **2009**, *80*, 014102.
[35] R. Tenne, *Nat. Nanotechnol.* **2006**, *21*, 2726.
[36] N. Illyaskutty, S. Sreedhar, H. Kohler, R. Philip, V. Rajan, V. M. Pillai, *J. Phys. Chem. C* **2013**, *117*, 7818.
[37] J. Luo, H. Zhu, H. Fan, J. Liang, H. Shi, G. Rao, J. Li, Z. Du, Z. Shen, *J. Phys. Chem. C* **2008**, *112*, 12594.
[38] Q. An, J. Sheng, X. Xu, Q. Wei, Y. Zhu, C. Han, C. Niu, L. Mai, *New J. Chem.* **2014**, *38*, 2075.
[39] M. Aksit, B. C. Hoselton, H. J. Kim, D.-H. Ha, R. D. Robinson, *ACS Appl. Mater. Inter.* **2013**, *5*, 8998.
[40] C. O. Z. Topal, S. Tan, H. Lu, N. Leventis, A. K. Kalkan, *J. Phys. Chem. C* **2012**, *116*, 10186.
[41] I. Mjejri, N. Etteyeb, F. Sediri, *Mater. Res. Bull.* **2013**, *48*, 3335.
[42] T. Gilson, O. Bizri, N. Cheetham, *J. Chem. Soc., Dalton Trans.* **1973**, 291.
[43] J. Zhu, L. Cao, Y. Wu, Y. Gong, Z. Liu, H. E. Hoster, Y. Zhang, S. Zhang, S. Yang, Q. Yan, P. M. Ajayan, R. Vajtai, *Nano Lett.* **2013**, *13*, 5408.
[44] K. Zhu, X. Yan, Y. Zhang, Y. Wang, A. Su, X. Bie, D. Zhang, F. Du, C. Wang, G. Chen, *ChemPlusChem* **2014**, *79*, 447.
[45] M. Simões, Y. Mettan, S. Pokrant, A. Weidenkaff, *J. Phys. Chem. C* **2014**, *118*, 14169.
[46] G. T. Chandrappa, P. Chithaiah, S. Ashoka, J. Livage, *Inorg. Chem.* **2011**, *50*, 7421.
[47] F. Li, Y. Ding, P. Gao, X. Xin, Z. L. Wang, *Angew. Chem. Int. Ed.* **2004**, *43*, 5238.
[48] Y. Peng, A.-W. Xu, B. Deng, M. Antonietti, H. Cölfen, *J. Phys. Chem. B* **2006**, *110*, 2988.
[49] Y. Xia, Y. Xiong, B. Lim, S. E. Skrabalak, *Angew. Chem. Int. Ed.* **2009**, *48*, 60.
[50] D. Xia, Q. Xue, J. Xie, H. Chen, C. Lv, F. Besenbacher, M. Dong, *Small* **2010**, *6*, 2010.
[51] J. W. Kim, V. Augustyn, B. Dunn, *Adv. Energy Mater.* **2012**, *2*, 141.
[52] L. Wang, X. He, W. Sun, J. Wang, Y. Li, S. Fan, *Nano Lett.* **2012**, *12*, 5632.
[53] H. Wu, G. Chan, J. W. Choi, Y. Yao, M. T. McDowell, S. W. Lee, A. Jackson, Y. Yang, L. Hu, Y. Cui, *Nat. Nanotechnol.* **2012**, *7*, 310.
[54] Y. Zhao, J. Feng, X. Liu, F. Wang, L. Wang, C. Shi, L. Huang, X. Feng, X. Chen, L. Xu, M. Yan, Q. Zhang, X. Bai, H. Wu, L. Mai, *Nat. Commun.* **2014**, *5*, 4565.